JOURNAL OF GUIDANCE, CONTROL, AND DYNAMICS
Vol. 27, No. 4, July–August 2004

Solar Sail Attitude Control and Dynamics, Part 2

Bong Wie*
Arizona State University, Tempe, Arizona 85287-6106

Dynamical models and attitude control concepts are developed for the purpose of sailcraft attitude control systems design. Particular emphasis is placed on a two-axis gimbaled control boom to counter the significant solar-pressure disturbance torque caused by an uncertain offset between the center of mass and center of pressure. Controlling sailcraft attitude by sail shifting and tilting is also investigated. A flight experiment in a geostationary orbit for the purpose of validating the principle of solar sailing is also proposed. A 40 × 40 m, 160-kg sailcraft in an Earth-centered elliptic orbit, with a nominal solar-pressure force of 0.01 N, an uncertain center-of-mass/center-of-pressure offset of ±0.1 m, and moments of inertia of (6000, 3000, 3000) kg · m^2, is studied to illustrate the various concepts and principles involved in dynamic modeling and attitude control design.

I. Introduction

THE technical challenges and issues associated with solar sailing, sail membranes and booms, sail packaging, boom deployment, and attitude control are discussed in Refs. 1 and 2 for a sail flight validation experiment previously proposed for the New Millennium Program Space Technology 7 (NMP ST7). A 40×40 m sailcraft configuration and its system architecture, as illustrated in Fig. 1, have been developed by the Jet Propulsion Laboratory (JPL) and AEC-Able Engineering for the NMP ST7 flight validation mission. A significant feature of this baseline ST7 sailcraft is the use of a two-axis gimbaled control boom, instead of control vanes, for propellantless sail-attitude control. Although the proposed solar sail mission was not selected as an actual flight validation mission of the NMP ST7, a 20-m scaled model of the baseline ST7 sailcraft is currently under development by NASA and AEC-Able Engineering for a ground validation experiment in 2005 (Ref. 3). A sail-attitude-control system employing a two-axis gimbaled control boom is also being further developed for a ground validation experiment on AEC-Able's 20-m sail in 2005 through the NASA In-Space Propulsion Solar Sail Program (Ref. 3).

In this paper, a 40×40 m, 160-kg sailcraft with a nominal solar-pressure force of 0.01 N, an uncertain center-of-mass/center-of-pressure (cm/cp) offset of ± 0.1 m, and moments of inertia of (6000, 3000, 3000) kg · m^2 is further studied to illustrate the various concepts and principles involved in dynamic modeling and attitude-control design. Particular emphasis is placed on various control-design options for countering the significant solar-pressure disturbance torque caused by an uncertain cm/cp offset. An overview of solar sail attitude control issues, as well as a simple spin-stabilization approach, was presented in Part 1 (Ref. 4).

The remainder of this paper is outlined as follows. Section II presents dynamic models and an attitude control problem for a sailcraft equipped with a gimbaled control boom and control vanes. In Sec. III, a gimbaled thrust-vector control (TVC) design problem is formulated for a sailcraft with a two-axis gimbaled control boom, and preliminary TVC design results are presented. In Sec. IV, a sailcraft controlled by shifting and tilting sail panels is investigated, and a flight experiment in a geostationary orbit for the purpose of validating the principle of solar sailing is also described.

Received 3 June 2002; presented as Paper 2002-4573 at the AIAA Guidance, Navigation, and Control Conference, Monterey, CA, 2–6 August 2002; revision received 25 August 2003; accepted for publication 3 November 2003.

*Professor, Department of Mechanical & Aerospace Engineering; bong.wie@asu.edu. Associate Fellow AIAA.

II. Sailcraft with a Gimbaled Control Boom and Control Vanes

As discussed in Part 1 (Ref. 4), one method of controlling the attitude of a three-axis stabilized sailcraft is to change its center-of-mass location relative to its center-of-pressure location. This can be achieved by articulating a control boom with a tip-mounted mass. Another method is to employ small reflective control vanes mounted at the spar tips. A dynamic model of a generic three-axis stabilized sailcraft with such tip-mounted vanes and a control boom, as illustrated in Fig. 2, is developed here. The complexity of the modeling and control problem inherent in even such a simple rigid sail, but with a moving mass, will be discussed.

The problem of a rigid spacecraft with internal moving mass was first investigated in the early 1960s. For spacecraft dynamical problems with internal moving mass, one may choose the composite center of mass of the total system as a reference point for the equations of motion. This formulation leads to a time-varying inertia matrix of the main rigid body, because the reference point is not fixed at the main body as the internal mass moves relative to the main body. On the other hand, one may choose the center of mass of the main body as the reference point, which leads to a constant inertia matrix of the main body relative to the reference point, but results in complex equations of motion.

In this paper, the second approach, choosing the center of mass of the main body as the reference point, is employed.

A. Dynamical Equations of Motion

Consider an ideal sailcraft model consisting of a rigid sail subsystem of mass m_s and a payload/bus of mass m_p located at the end of a massless control boom of length l, as shown in Fig. 2. The origin of the body-fixed reference frame (x, y, z) is located at point O, which is assumed to be the center of mass of a rigid sail subsystem of mass m_s.

The position vector of the payload/bus mass from the reference point O is expressed as

$$\boldsymbol{r} = x\boldsymbol{i} + y\boldsymbol{j} + z\boldsymbol{k} = l\boldsymbol{e}_r = l(\cos\phi\boldsymbol{i} + \sin\phi\cos\theta\boldsymbol{j} + \sin\phi\sin\theta\boldsymbol{k}) \quad (1)$$

where ϕ is the boom tilt angle and θ is the boom azimuth angle relative to the sailcraft body axes (x, y, z). These two gimbal angles can be considered as control inputs; however, the gimbal dynamics needs to be included later for detailed control design.

There are four different ways to model the attitude dynamics of a spacecraft with a moving mass. In general, the four different angular momentum equations are given by

$$\dot{\boldsymbol{H}}_o + \dot{\boldsymbol{R}}_o \times m\dot{\boldsymbol{r}}_c = \boldsymbol{M}_o \quad (2a)$$

$$\dot{\boldsymbol{h}}_o + \boldsymbol{r}_c \times m\boldsymbol{a}_o = \boldsymbol{M}_o \quad (2b)$$

$$\dot{\boldsymbol{H}}_c + \boldsymbol{r}_c \times m\boldsymbol{a}_c = \boldsymbol{M}_o \quad (2c)$$

$$\dot{\boldsymbol{H}}_c = \boldsymbol{M}_c \quad (2d)$$

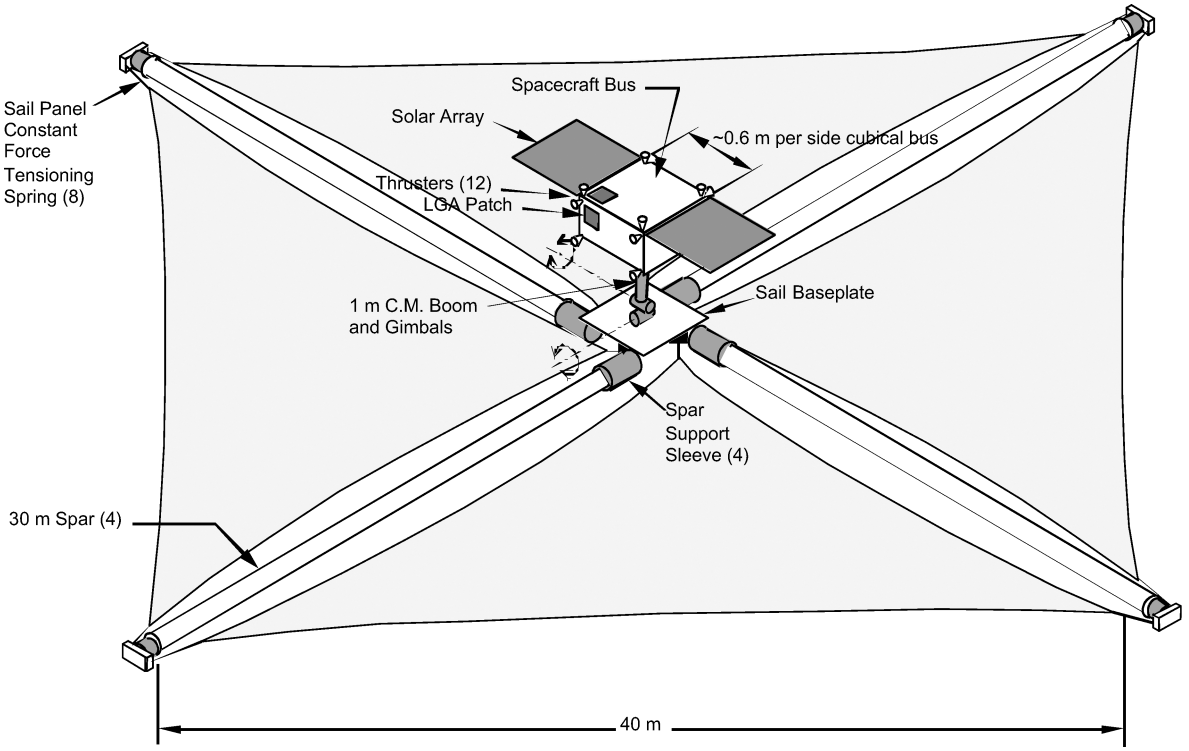

Fig. 1 A 40 × 40 m, 160-kg sailcraft configuration (not to scale), designed by JPL and AEC-Able Engineering for the New Millennium Program Space Technology 7 sail flight experiment (Refs. 1, 2).

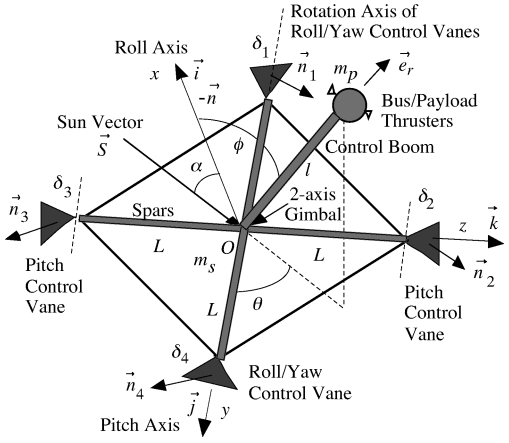

Fig. 2 Three-axis stabilized square sailcraft with a two-axis gimbaled control boom and four tip-mounted control vanes.

where m is the total system mass, $\boldsymbol{H}_o$ and $\boldsymbol{h}_o$ are, respectively, the absolute and relative angular momentum about an arbitrary reference point O, $\boldsymbol{a}_o$ is the absolute acceleration of the point O, $\boldsymbol{a}_c$ is the absolute acceleration of the composite center of mass, $\boldsymbol{H}_c$ is the absolute angular momentum about the composite center of mass, $\boldsymbol{M}_o$ is the moment of the external forces about the point O, and $\boldsymbol{M}_c$ is the moment of the external forces about the composite center of mass.

An inertially fixed point or the moving center of mass is often selected as a reference point O. However, there are many cases in which a reference point is selected to be neither inertially fixed nor the center of mass of the system.

For a sailcraft with a gimbaled control boom, one may choose an angular momentum equation of the form

$$\dot{\boldsymbol{h}}_o + m\boldsymbol{r}_c \times \boldsymbol{a}_o = \boldsymbol{M}_o \tag{3}$$

where $\boldsymbol{h}_o$ is the relative angular momentum of the total system about point O, $m = m_s + m_p$ is the total mass, $\boldsymbol{r}_c$ is the position vector of the composite center of mass from the reference point O, $\boldsymbol{a}_o$ is the inertial acceleration of the point O, and $\boldsymbol{M}_o$ is the external torque vector about the point O. The position vector of the composite center of mass is simply given by

$$\boldsymbol{r}_c = m_p/(m_s + m_p)\boldsymbol{r} = (m_p/m)l\boldsymbol{e}_r \tag{4}$$

The relative angular momentum of the total system about point O is given by

$$\boldsymbol{h}_o = \hat{J} \cdot \boldsymbol{\omega} + m_p \boldsymbol{r} \times \dot{\boldsymbol{r}} \tag{5}$$

where $\hat{J}$ is the inertia dyadic of the system and $\boldsymbol{\omega}$ is the angular velocity vector of the main body (i.e., sail subsystem), expressed as

$$\boldsymbol{\omega} = \omega_x \boldsymbol{i} + \omega_y \boldsymbol{j} + \omega_z \boldsymbol{k} \tag{6}$$

The inertia dyadic of the system, including the payload mass, about the reference point O is given by

$$\hat{J} = [\boldsymbol{i} \quad \boldsymbol{j} \quad \boldsymbol{k}] \begin{bmatrix} J_{11} & J_{12} & J_{13} \\ J_{21} & J_{22} & J_{23} \\ J_{31} & J_{32} & J_{33} \end{bmatrix} \begin{bmatrix} \boldsymbol{i} \\ \boldsymbol{j} \\ \boldsymbol{k} \end{bmatrix}$$

where $J_{11} = J_x + m_p(y^2 + z^2)$, $J_{22} = J_y + m_p(x^2 + z^2)$, $J_{33} = J_z + m_p(x^2 + y^2)$, $J_{12} = J_{21} = -m_p xy$, $J_{13} = J_{31} = -m_p xz$, $J_{23} = J_{32} = -m_p yz$, and (J_x, J_y, J_z) are the principal moments of inertia of the sail subsystem, not including the tip mass m_p.

As discussed in Part 1 (Ref. 4), the resultant solar-radiation pressure (SRP) force can be simply modeled as

$$\boldsymbol{F} = \eta P A(\boldsymbol{S} \cdot \boldsymbol{n})^2 \boldsymbol{n} = F_s \cos^2\alpha \boldsymbol{n} \tag{7}$$

where η is the overall sail-thrust coefficient ($\eta_{\max} = 2$), $P = 4.563 \times 10^{-6}$ N/m^2, A is the total sail area, $F_s \equiv \eta P A$ is the maximum sail thrust, $\boldsymbol{S}$ is a unit vector from the sun, and $\boldsymbol{n} \equiv -\boldsymbol{i}$ is the unit vector normal to the sail surface. The resultant SRP force, nominally acting on the reference point O but with a possible uncertain offset, generates a control torque about the composite center of mass.

In addition to the gimbaled control boom, two or four vanes at the spar tips can be used, each vane with one or two degrees of freedom. Control vanes, each with two degrees of freedom, provide more control redundancy and also more control authority. A variety of

control vane configurations for generating proper three-axis control torques are possible. An arrangement of four triangular vanes, as illustrated in Fig. 2, is considered here without loss of generality. The SRP control force acting on a triangular control vane acts at a point two-thirds of the distance out on the spar axis, called the vane center of pressure.

The control-torque vector about the point O generated by deflecting the four control vanes is expressed as

$$\boldsymbol{M}_o = \sum_{i=1}^{4} \boldsymbol{l}_i \times F_c(\boldsymbol{S}\cdot\boldsymbol{n}_i)^2\boldsymbol{n}_i \tag{8}$$

where $F_c = \eta P A_c$, A_c is the control-vane area, with all vanes assumed identical, $\boldsymbol{l}_i$ is the position vector of the ith vane center of pressure from the point O, and

$$\boldsymbol{n}_1 = -\cos\delta_1\boldsymbol{i} - \sin\delta_1\boldsymbol{k}, \qquad \boldsymbol{n}_2 = -\cos\delta_2\boldsymbol{i} + \sin\delta_2\boldsymbol{k}$$

$$\boldsymbol{n}_3 = -\cos\delta_3\boldsymbol{i} + \sin\delta_3\boldsymbol{k}, \qquad \boldsymbol{n}_4 = -\cos\delta_4\boldsymbol{i} - \sin\delta_4\boldsymbol{k}$$

The inertial acceleration of the reference point O is related to the inertial acceleration of the composite center of mass as

$$\boldsymbol{a}_o = \boldsymbol{a}_c - \ddot{\boldsymbol{r}}_c$$

$$= \frac{1}{m}\left[F_s\cos^2\alpha\boldsymbol{n} + \sum_{i=1}^{4} F_c(\boldsymbol{S}\cdot\boldsymbol{n}_i)^2\boldsymbol{n}_i\right] - \frac{m_p}{m}\ddot{\boldsymbol{r}} \tag{9}$$

The attitude equation of motion, (3), can then be rewritten as

$$\frac{d}{dt}(\hat{J}\cdot\boldsymbol{\omega} + m_p\boldsymbol{r}\times\dot{\boldsymbol{r}}) + \frac{m_p}{m}\boldsymbol{r}$$

$$\times\left\{\left[F_s\cos^2\alpha\boldsymbol{n} + \sum_{i=1}^{4} F_c(\boldsymbol{S}\cdot\boldsymbol{n}_i)^2\boldsymbol{n}_i\right] - m_p\ddot{\boldsymbol{r}}\right\}$$

$$= \sum_{i=1}^{4} \boldsymbol{l}_i \times F_c(\boldsymbol{S}\cdot\boldsymbol{n}_i)^2\boldsymbol{n}_i \tag{10}$$

where $\boldsymbol{r} = x\boldsymbol{i} + y\boldsymbol{j} + z\boldsymbol{k}$. The complexity of the equations of motion, caused by the time-varying center-of-mass location, can be seen in Eq. (10).

Considering the rotational equations of motion about the composite center of mass, instead of the body-fixed reference point O, we obtain the following equations of motion:

$$J_x\dot{\omega}_x + \cdots = F_c\cos^2\alpha\left(l_1\cos^2\delta_1\sin\delta_1 - l_4\cos^2\delta_4\sin\delta_4\right) \tag{11}$$

$$J_y\dot{\omega}_y + \cdots = (m_p/m)F_s l\cos^2\alpha\sin\phi\sin\theta$$

$$+ F_c\left[-l_2\cos^2(\alpha-\delta_2)\cos\delta_2 + l_3\cos^2(\alpha-\delta_3)\cos\delta_3\right] \tag{12}$$

$$J_z\dot{\omega}_z + \cdots = -(m_p/m)F_s l\cos^2\alpha\sin\phi\cos\theta$$

$$- F_c\cos^2\alpha\left(l_1\cos^3\delta_1 - l_4\cos^3\delta_4\right) \tag{13}$$

where $(\omega_x, \omega_y, \omega_z)$ are the angular velocity components and (J_x, J_y, J_z) are the moments of inertia of the total system about the composite center of mass, which are functions of gimbal angles ϕ and θ. Furthermore, the distance from the composite center of mass to each vane, l_i, is also a function of ϕ and θ. There are also additional terms on the left-hand sides of these equations, which are caused by the time-varying inertias and gyroscopic couplings. The complexity of a dynamic model caused by the time-varying center-of-mass location is evident here again.

B. Sailcraft with Control Vanes

For a sailcraft with control vanes (but without a gimbaled control boom), we have the following equations of motion:

$$J_x\dot{\omega}_x = F_c L\cos^2\alpha\left(\cos^2\delta_1\sin\delta_1 - \cos^2\delta_4\sin\delta_4\right) \tag{14}$$

$$J_y\dot{\omega}_y = F_c L\left[-\cos^2(\alpha-\delta_2)\cos\delta_2 + \cos^2(\alpha-\delta_3)\cos\delta_3\right] \tag{15}$$

$$J_z\dot{\omega}_z = -F_c L\cos^2\alpha\left(\cos^3\delta_1 - \cos^3\delta_4\right) \tag{16}$$

where L is the distance from the center of mass to the center of pressure of each control vane ($\approx$ the spar length).

Given the desired control torques, (T_x, T_y, T_z), from an attitude control system, we have

$$T_x = F_c L\cos^2\alpha\left(\cos^2\delta_1\sin\delta_1 - \cos^2\delta_4\sin\delta_4\right)$$

$$\approx F_c L\cos^2\alpha(\delta_1 - \delta_4) \tag{17a}$$

$$T_y = F_c L\left[-\cos^2(\alpha-\delta_2)\cos\delta_2 + \cos^2(\alpha-\delta_3)\cos\delta_3\right] \tag{17b}$$

$$T_z = -F_c L\cos^2\alpha\left(\cos^3\delta_1 - \cos^3\delta_4\right) \approx F_c L\cos^2\alpha\left(\delta_1^2 - \delta_4^2\right)$$

$$\approx F_c L\cos^2\alpha(\delta_1 - \delta_4)(\delta_1 + \delta_4) \tag{17c}$$

Defining $\Delta = \delta_1 - \delta_4$ and $\Theta = \delta_1 + \delta_4$, we obtain the commanded roll/yaw control-vane angles as

$$\delta_{1c} = (\Delta_c + \Theta_c)/2 \tag{18a}$$

$$\delta_{4c} = (\Delta_c - \Theta_c)/2 \tag{18b}$$

where Δ_c and Θ_c are determined from (17) as

$$\Delta_c = T_x\Big/\left(F_c L\cos^2\alpha\right) \tag{19a}$$

$$\Theta_c = T_z/T_x \qquad \text{if} \qquad T_x \neq 0 \tag{19b}$$

When $T_x = 0$, the above vane-steering logic has a singularity problem. That is, the yaw torque cannot be generated when $\delta_1 = \delta_4$ for $T_x = 0$. This is the main reason for requiring additional flaps, mounted on the outermost solar panels, for the OTS, TELECOM 1, and INMARSAT 2 satellites, as discussed in Part 1 (Ref. 4).

Because there exists a solution, $\delta_1 \neq \delta_4$, of the nonlinear equations

$$\cos^2\delta_1\sin\delta_1 - \cos^2\delta_4\sin\delta_4 = 0 \tag{20a}$$

$$\cos^3\delta_1 - \cos^3\delta_4 = -T_z\Big/\left(F_c L\cos^2\alpha\right) \tag{20b}$$

it is also possible to generate an imbalance in yaw torque without inducing a roll-axis windmill torque. However, actual implementation of this method will require further detailed study.

C. Statically Stable Sailcraft

An interplanetary spacecraft is often said to be statically stable when its center of mass lies between the sun and its center of pressure, as illustrated in Fig. 3. Whenever a statically stable sailcraft rotates away from its neutral sun-pointing orientation, a restoring (stabilizing) torque is generated. The dynamical behavior such a statically stable sailcraft is analogous to that of a gravity-gradient-stabilized satellite. That is, if disturbed, the sailcraft will oscillate indefinitely. If the center of pressure lies between the sun and the center of mass, a destabilizing torque is generated whenever the sailcraft rotates away from its null or trim orientation.

Consider a simple pitch-axis model of a sailcraft with control vanes, as illustrated in Fig. 3. The pitch-axis equation of motion becomes

$$J_y\ddot{\alpha} = F_c L\left[-\cos^2(\alpha-\delta_2)\cos\delta_2 + \cos^2(\alpha-\delta_3)\cos\delta_3\right]$$

$$- m_s/(m_s+m_p)(b+l)F_t \approx F_c L\left[-\cos^3\delta_2 - 2\left(\cos^2\delta_2\sin\delta_2\right)\right.$$

$$\left.+ \cos^3\delta_3 + 2\left(\cos^2\delta_3\sin\delta_3\right)\alpha\right] - m_s/(m_s+m_p)(b+l)F_t \tag{21}$$

where J_y is the pitch moment of inertia of the complete system.

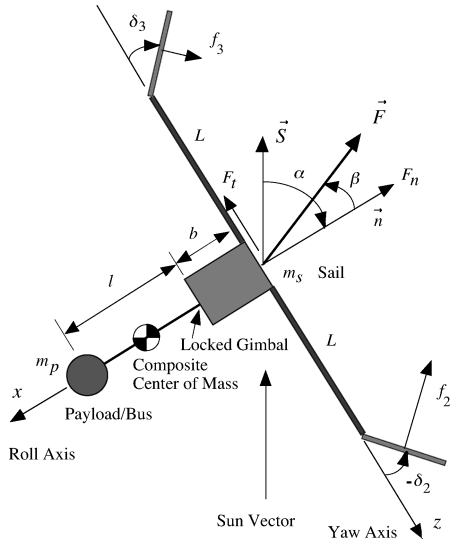

Fig. 3 Pitch-axis model of a statically stable sailcraft.

For fixed control vane angles of $\delta = -\delta_2 = \delta_3 > 0$, we have a pitch-axis dynamical model of the form

$$\ddot{\alpha} + \omega_n^2 \alpha = 0 \tag{22}$$

where

$$\omega_n^2 = \frac{1}{J_y}\left[4F_c L\cos^2\delta\sin\delta + \frac{m_p(b+l)}{m_s+m_p}PA(1-\rho_s)\right]$$

A 76×76 m square sailcraft is currently under development by Team Encounter and L'Garde (Refs. 3 and 4 of Part I), and its sun-pointing orientation is passively stabilized by means of trim tabs, as discussed here.

III. Gimbaled TVC Design for a Sailcraft

A simplified pitch-axis model of the baseline ST7 sailcraft is illustrated in Fig. 4. The sailcraft consists of a sail subsystem and a payload/bus system. The sail subsystem is treated as a gimbaled engine, and a gimbaled TVC design problem is formulated here for the ST7 sailcraft.

A. Pitch-Axis Dynamical Model

The equations of motion of the gimbaled two-body system shown in Fig. 4 can be obtained as

$$m_s a_x = G_x - F_n \tag{23a}$$

$$m_s a_z = G_z - F_t \tag{23b}$$

$$m_p\left[a_x - b\dot{\alpha}^2 - l(\ddot{\alpha}+\ddot{\delta})\sin\delta - l(\dot{\alpha}+\dot{\delta})^2\cos\delta\right] = -G_x - f\sin\delta \tag{23c}$$

$$m_p\left[a_z - b\ddot{\alpha} - l(\ddot{\alpha}+\ddot{\delta})\cos\delta + l(\dot{\alpha}+\dot{\delta})^2\sin\delta\right] = -G_z - f\cos\delta \tag{23d}$$

$$J_s\ddot{\alpha} = -bG_z - T_g + T_{\text{ext}} \tag{23e}$$

$$J_p(\ddot{\alpha}+\ddot{\delta}) = T + T_g - G_x l\sin\delta - G_z l\cos\delta \tag{23f}$$

where (a_x, a_z) are the body-axis components of the sail-subsystem center-of-mass acceleration; (G_x, G_z) the body-axis components of the gimbal-joint reaction force; δ the gimbal angle; α the sail pitch (sun) angle; m_s and J_s the mass and pitch inertia of the sail subsystem, respectively; (F_n, F_t) the normal and transverse components of total solar-pressure force; m_p and J_p the payload/bus system mass and inertia, respectively; l the control-boom length; b the distance between the sail subsystem center of mass and the gimbal joint; T_g the gimbal (internal) control torque; T the control torque from a pitch reaction wheel located at the payload/bus system; and f the reaction-jet force.

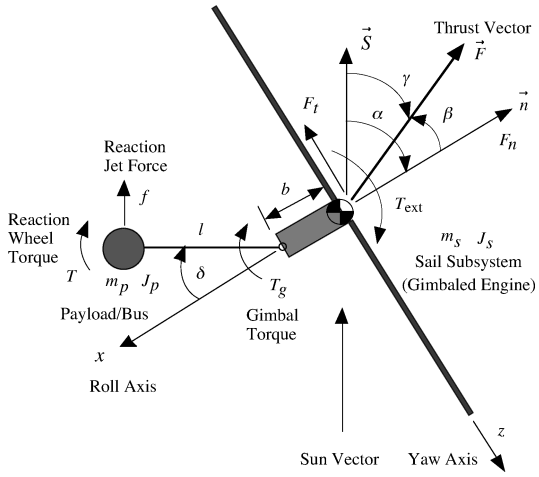

Fig. 4 Simplified pitch-axis model of the ST7 sailcraft controlled by a gimbaled TVC system, reaction wheels, and/or reaction jets.

The external disturbance torque, T_{ext}, in Eq. (23e) consists of the solar-pressure disturbance torque and the gravity-gradient torque as follows:

$$T_{\text{ext}} = \epsilon F_n + 3\mu/r^3(J_x - J_z)\sin(\alpha-\theta)\cos(\alpha-\theta) \tag{24}$$

where ϵ is the cm/cp offset of the sail subsystem along the yaw axis, μ the Earth's gravitational parameter, (J_x, J_z) the roll and yaw moments of inertia of the sail subsystem, r the radial distance of the sailcraft from the center of the Earth, and θ the true anomaly. The gravity-gradient torque of the form in Eq. (24) was derived in Part 1 (Ref. 4).

Eliminating G_x and G_z from Eqs. (23), we obtain

$$m_s a_x = -m_p\left[a_x - b\dot{\alpha}^2 - l(\ddot{\alpha}+\ddot{\delta})\sin\delta - l(\dot{\alpha}+\dot{\delta})^2\cos\delta\right] - f\sin\delta - F_n \tag{25a}$$

$$m_s a_z = -m_p\left[a_z - b\ddot{\alpha} - l(\ddot{\alpha}+\ddot{\delta})\cos\delta + l(\dot{\alpha}+\dot{\delta})^2\sin\delta\right] - f\cos\delta - F_t \tag{25b}$$

$$J_s\ddot{\alpha} = -b(m_s a_z + F_t) - T_g + T_{\text{ext}} \tag{25c}$$

$$J_p(\ddot{\alpha}+\ddot{\delta}) = -(m_s a_x + F_n)l\sin\delta - (m_s a_z + F_t)l\cos\delta + T + T_g \tag{25d}$$

For small angles and rates, we obtain the following set of linearized equations of motion:

$$(m_s+m_p)a_x = -f\delta - F_n \tag{26a}$$

$$(m_s+m_p)a_z = m_p[b\ddot{\alpha} + l(\ddot{\alpha}+\ddot{\delta})] - f - F_t \tag{26b}$$

$$J_s\ddot{\alpha} = -b(m_s a_z + F_t) - T_g + T_{\text{ext}} \tag{26c}$$

$$J_p(\ddot{\alpha}+\ddot{\delta}) = -(m_s a_x + F_n)l\delta - (m_s a_z + F_t)l + T + T_g \tag{26d}$$

Eliminating a_x and a_z gives

$$[J_s + (m_s m_p/m)b(b+l)]\ddot{\alpha} + (m_s m_p/m)bl\ddot{\delta} = -(m_p/m)bF_t + (m_s/m)bf - T_g + T_{\text{ext}} \tag{27a}$$

$$[J_p + (m_s m_p/m)l(b+l)]\ddot{\alpha} + [J_p + (m_s m_p/m)l^2]\ddot{\delta} = -(m_p/m)lF_t - (m_p/m)lF_n\delta + (m_s/m)lf + T_g + T \tag{27b}$$

where $m = m_s + m_p$. As discussed in Part 1 (Ref. 4), the solar-radiation-pressure force components (F_n, F_t) can be expressed either as

$$F_n = PA\left\{(1+\rho_s)\cos^2\alpha + \tfrac{2}{3}\rho_d \cos\alpha\right\} \tag{28a}$$

$$F_t = PA(1-\rho_s)\cos\alpha\sin\alpha \tag{28b}$$

or as

$$F_n = PA\left[(1+rs)\cos^2\alpha + B_f r(1-s)\cos\alpha + \frac{e_f B_f - e_b B_b}{e_f + e_b}(1-r)\cos\alpha\right] \tag{29a}$$

$$F_t = PA(1-rs)\cos\alpha\sin\alpha \tag{29b}$$

B. Preliminary TVC Design and Simulation Results

A baseline configuration is assumed as $m_s = 40$ kg, $m_p = 120$ kg, $b = 0.5$ m, $\epsilon = \pm 0.1$ m, $l = 2$ m, $J_s = 3000$ kg $\cdot$ m^2, $J_x = 6000$ kg $\cdot$ m^2, $J_z = 3000$ kg $\cdot$ m^2, $J_p = 20$ kg $\cdot$ m^2, $P = 4.563 \times 10^{-6}$ N/m^2, and $A = 1400$ m^2. More detailed mass properties and basic characteristics of this 40×40 m sailcraft are summarized in Table 1. The following optical properties are also assumed: $B_f = 0.79$, $B_b = 0.55$, $e_f = 0.05$, $e_b = 0.55$, $r = 0.88$, and $s = 0.94$.

An elliptic orbit, called the supersynchronous transfer orbit (SSTO), chosen for the ST7 sail validation mission is characterized as

$$r_p = 6374 + 2000 = 8374 \text{ km}$$

$$r_a = 6374 + 78{,}108 = 84{,}482 \text{ km}$$

$$a = (r_p + r_a)/2 = 46{,}428 \text{ km}$$

$$e = (r_a - r_p/r_a + r_p) = 0.8196$$

$$i = 12 \text{ deg (from the ecliptic plane)}$$

$$p = a(1-e^2) = 15{,}238 \text{ km}$$

$$n = \sqrt{\mu/a^3} = 6.311 \times 10^{-5} \text{ rad/s}$$

and has an orbital period of 27.65 h.

A linear state-space model for control design can be obtained as

$$\frac{d}{dt}\begin{bmatrix}\alpha\\ \dot\alpha\\ \delta\\ \dot\delta\end{bmatrix} = \begin{bmatrix}0 & 1 & 0 & 0\\ -1.9705\times10^{-8} & 0 & 1.2316\times10^{-6} & 0\\ 0 & 0 & 0 & 1\\ -1.1803\times10^{-5} & 0 & -1.2470\times10^{-4} & 0\end{bmatrix}\begin{bmatrix}\alpha\\ \dot\alpha\\ \delta\\ \dot\delta\end{bmatrix} + \begin{bmatrix}0\\ -4.0462\times10^{-4}\\ 0\\ 7.6342\times10^{-3}\end{bmatrix} T_g$$

with open-loop eigenvalues of $\pm 0.0112\,j$ and $\pm 0.0004\,j$. We may then employ a gimbal control logic of the form

$$T_g = -K_\alpha(\alpha - \alpha_c) - K_i\int(\alpha - \alpha_c) - K_{\dot\alpha}\dot\alpha - K_\delta\delta - K_{\dot\delta}\dot\delta \tag{30}$$

where $(K_\alpha, K_i, K_{\dot\alpha}, K_\delta, K_{\dot\delta})$ are feedback control gains and α_c is the commanded pitch (sun) angle. A linear–quadratic-regulator (LQR) design technique was used to determine a set of control gains $(K_\alpha, K_i, K_{\dot\alpha}, K_\delta, K_{\dot\delta})$, resulting in the following closed-loop eigenvalues: $-0.23 \pm j0.23$, $-.0009 \pm j0.0012$, and -0.0002. The feasibility of employing a gimbaled control system for a 35-deg pitch maneuver with an initial pitch rate of -0.05 deg/s in the presence of a disturbance torque caused by a cm/cp offset of ± 0.1 m is demonstrated in Fig. 5. Certain variables such as the pitch rate, gimbal rate, and gimbal torque are shown in Fig. 5 for the initial 55-s period to indicate their peak values.

Table 1 ST7 sailcraft characteristics

Characteristic	Value
Sail film	$m_f = 6.1$ kg
Booms (4×)	$m_b = 4 \times 3.575 = 14.3$ kg
	$EI \approx 1000$–2000 N $\cdot$ m^2
	$L = 30$ m
	$\rho = 0.1191$ kg/m
Hub platform	$m_h = 19.6$ kg
Solar sail	$m_s = m_f + m_b + m_h = 40$ kg
Payload/bus	$m_p = 116$ kg
Total mass	$m = m_s + m_p = 156$ kg
Sail area	$A = 1400$ m^2
Solar pressure	$P = 4.563$ e-6 N/m^2
Thrust coefficient	$\eta = 1.816$ (ideal $\eta_{\max} = 2$)
Maximum thrust	$F_{\max} = \eta PA = 0.0116$ N
Area-to-mass ratio	$A/m = 8.97$ m^2/kg
Areal density	$\sigma = m/A = 0.111$ kg/m^2
Acceleration	$a_c = F_{\max}/m = \eta PA/m$
	$= \eta P/\sigma = 73.7$ e-6 m/s^2

Figure 6 shows simulation results for the ST7 sailcraft during sun-pointing mode operation in two consecutive orbits for the desired sun angle of $\alpha = 0$ deg. The simulation results demonstrate the overall effectiveness and practicality of a gimbaled control system for the ST7 sailcraft in the presence of the solar-pressure and gravity-gradient torques. The effect of the gravity-gradient disturbance torque on the pitching motion of the ST7 during its perigee passage is evident in this figure.

Further detailed control-design tradeoffs are needed to select a proper control bandwidth in the presence of mission/hardware constraints (e.g., pointing accuracy, sail-turning rate, maximum gimbal torque, maximum gimbal angle, maximum gimbal rate, gimbal friction, sail structural flexibility). Furthermore, a complete three-axis simulation validation of a two-axis TVC design needs to be performed in a further detailed study.

IV. Attitude Control by Shifting and Tilting Sail Panels

In this section, a somewhat unconventional way of controlling the attitude of a sailcraft by shifting (translating) and tilting (rotating) sail panels is introduced.

A. Shifting and Tilting Sail Panels

The sailcraft configuration shown in Fig. 7 was proposed by JPL for the New Millennium Program Space Technology 6 (ST6) mission. As illustrated in Fig. 7, this sailcraft configuration has four triangular sail panels supported between the four booms. A significant feature of this configuration is that the outer two corners of each sail panel are attached by constant-force springs to spreader bars at the end of the booms. The inner corner of the sail is attached to a tether that feeds from a spool with an actuator. The sail panel can be radially translated inboard or outboard by reeling in or paying out the inboard tether from the spool. This moves the center of pressure in or out for pitch/yaw control, while each sail panel area is kept constant.

Additionally, each boom can be rotated at the base about its long axis. This twists the spreader bars at the end of the booms out of the plane for the sail. This, in turn, lifts or lowers the outer corners of the sail panels out of plane and can be used for roll control. If each boom is rotated clockwise at the base (as viewed from the sail hub) the sail panels will form a pinwheel and provide a roll-axis windmill torque to the sail.

Because of uncertainties associated with manufacture, mechanization, and deployment of such translating/tilting sail panels, an uncertain cm/cp offset of ± 0.25 m, instead of ± 0.1 m, is assumed here for the 40×40 m sailcraft shown in Fig. 7.

The study objective for this type of sailcraft was to develop an innovative propellantless attitude control subsystem, develop attitude control algorithms, and validate the concept of airplane-like control of a sailcraft using control surfaces such as ailerons, elevators, and rudder, as illustrated in Fig. 8.

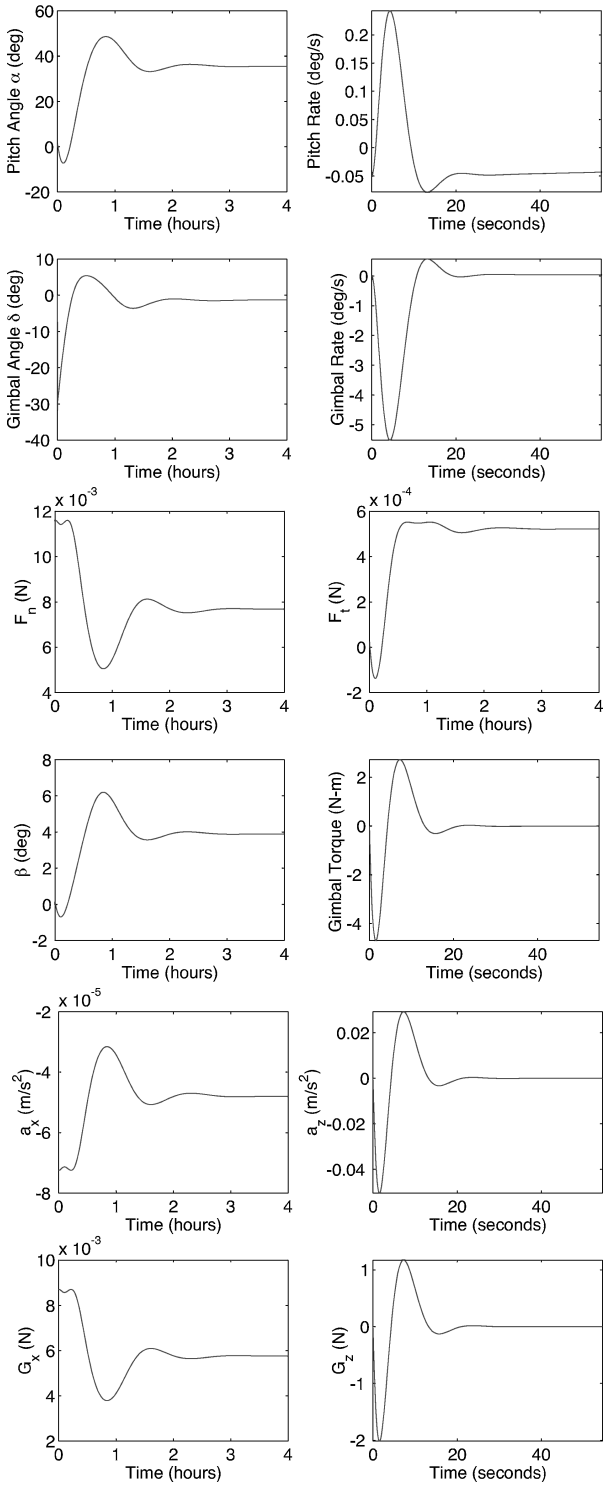

Fig. 5 Pitch-axis control simulation results for the ST7 sailcraft controlled by a gimbaled TVC system ($\alpha_c = 35$ deg, $\epsilon = 0.1$ m, and initial pitch rate = -0.05 deg/s).

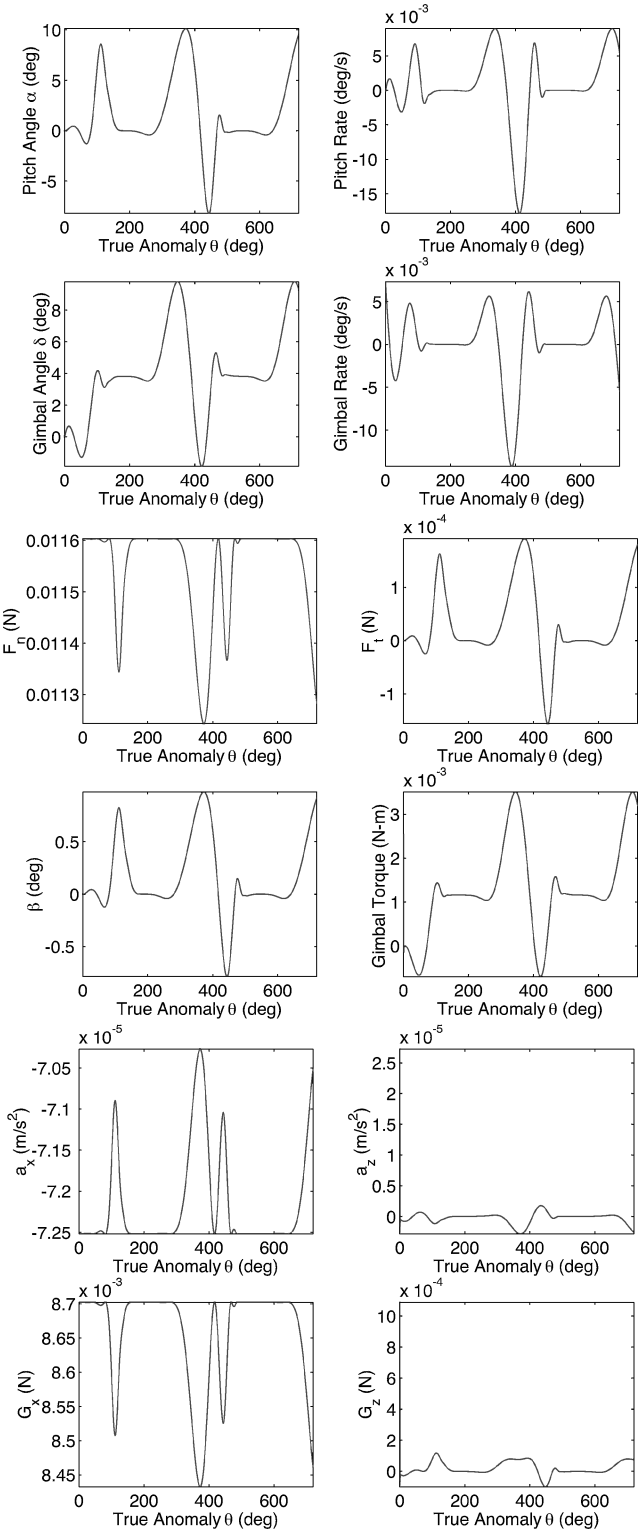

Fig. 6 Sun-pointing mode simulation results for the ST7 sailcraft in a supersynchronous transfer orbit ($\alpha_c = 0$ deg, $\epsilon = 0.1$ m).

B. Dynamical Models

A set of simplified dynamic models are provided here for the purpose of preliminary control design and computer simulation.

1. *Attitude Dynamical Equations*

The equations of motion of a sun-pointing spacecraft with small roll and yaw angles in an Earth-centered elliptic orbit are given by (Part 1)

$$J_x\ddot{\theta}_x + [\dot{\theta}^2 + (3\mu/r^3)\cos^2\theta_y](J_y - J_z)\theta_x + 3\mu/r^3(J_y - J_z)(\sin\theta_y\cos\theta_y)\theta_z = T_x \tag{31a}$$

$$J_y\ddot{\theta}_y + 3\mu/r^3(J_x - J_z)\sin\theta_y\cos\theta_y = J_y\ddot{\theta} + T_y \tag{31b}$$

$$J_z\ddot{\theta}_z + [\dot{\theta}^2 + (3\mu/r^3)\sin^2\theta_y](J_y - J_x)\theta_z + 3\mu/r^3(J_y - J_x)(\sin\theta_y\cos\theta_y)\theta_x = T_z \tag{31c}$$

where (x, y, z) are the body-fixed control axes, $(\theta_x, \theta_y, \theta_z)$ are the (roll, pitch, yaw) attitude angles, (T_x, T_y, Tz) are control torques generated by translating/tilting sail panels, θ is the true anomaly, and r is the orbital radius from the center of the Earth.

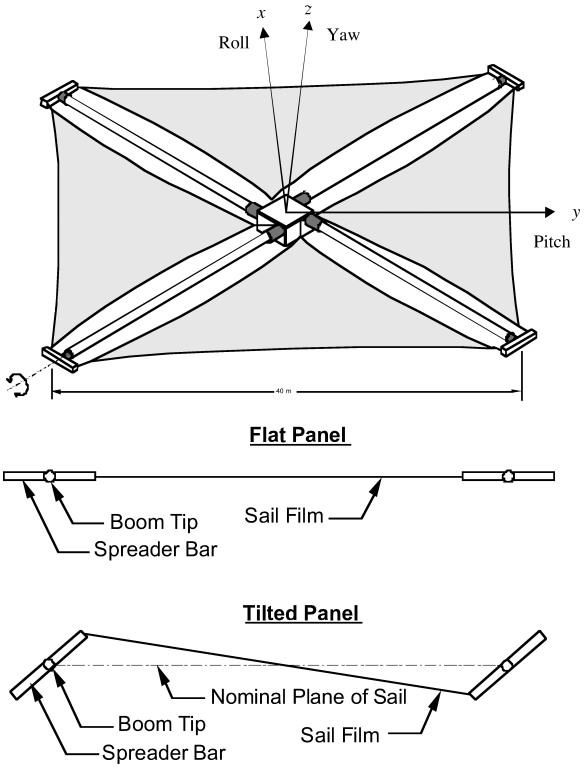

Fig. 7 A 40 × 40 m sailcraft and its attitude control mechanism, proposed by JPL for the NMP ST6 sail deployment and control validation experiment.

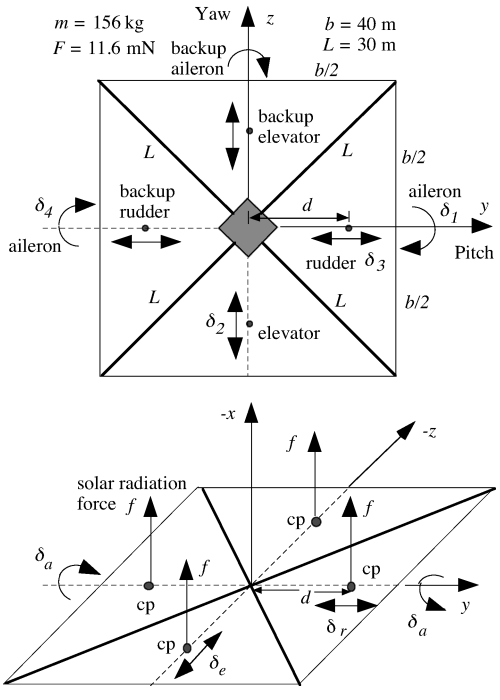

Fig. 8 Airplane-like attitude and flight control by shifting and tilting four sail panels.

The pitch angle relative to the local vertical local horizontal (LVLH) frame, θ_y, can be expressed as

$$\theta_y = \theta - \pi/2 + \alpha \tag{32}$$

where α is the sun angle between the surface normal and the sun-line. The pitch equation of motion of a sun-pointing sailcraft then becomes

$$J_y\ddot{\alpha} - 3\mu/r^3(J_x - J_z)\sin(\alpha-\theta)\cos(\alpha-\theta) = T_y \tag{33}$$

2. Orbital Equations in ECI (Earth-Centered Inertial) Coordinates

$$\ddot{X} = -\mu\frac{X}{r^3} - \frac{F\cos^2 i_\odot}{m}\cos\gamma \tag{34a}$$

$$\ddot{Y} = -\mu\frac{Y}{r^3} + \frac{F\cos^2 i_\odot}{m}\sin\gamma \tag{34b}$$

$$\ddot{Z} = -\mu\frac{Z}{r^3} + \frac{F\sin^2 i_\odot}{m} \tag{34c}$$

$$r = \sqrt{X^2+Y^2+Z^2} \tag{34d}$$

where (X, Y, Z) = satellite position in ECI coordinates; $F = 0.0116(0.349 + 0.662\cos 2\gamma - 0.011\cos 4\gamma)$; $\gamma = \alpha - \beta =$ thrust angle, as defined in Fig. 7 of Part 1; $\alpha =$ sun angle between the surface normal and the sun; $\beta =$ thrust offset due to nonflat sail surface; and $i_\odot =$ inclination angle from the ecliptic plane.

3. Control Torque Models

The nominal total thrust for an assumed value of $\eta = 1.816$ is estimated as $F_{\max} = 11.6$ mN. The thrust force generated by an individual panel is assumed to be $f = F_{\max}/4 = 2.9$ mN. As illustrated in Fig. 8, $\delta_1 = -\delta_4 = \delta_a$ are panel rotation angles for roll control, $\delta_2 = \delta_e$ is a panel displacement for pitch control, and $\delta_3 = \delta_r$ is a panel displacement for yaw control. Employing an ideal SRP model for control torques, we can obtain the roll, pitch, and yaw control torques (in units of N-m) generated by translating/tilting panels as follows:

$$T_x = (f\cos^2\alpha)d\left(\cos^2\delta_1\sin\delta_1 + \cos^2\delta_4\sin\delta_4\right)$$

$$= (f\cos^2\alpha)2d\cos^2\delta_a\sin\delta_a \quad \text{when} \quad \delta_1 = \delta_4 = \delta_a$$

$$\approx (0.0029)(2)(13.3)\delta_a \quad \text{for small} \quad \alpha, \delta_a$$

$$T_y = (f\cos^2\alpha)\delta_e \approx 0.0029\delta_e$$

$$T_z = (f\cos^2\alpha)\delta_r + (f\cos^2\alpha)d\left(\cos^3\delta_1 - \cos^3\delta_4\right)$$

$$\approx 0.0029\delta_r \quad \text{when} \quad \delta_1 = \delta_4$$

$$T_x = T_y = T_z = 0 \quad \text{when} \quad \alpha = 90^\circ \text{(control singularity)}$$

Control redundancy for each axis can be observed in Fig. 8. For example, if one sail panel with δ_e displacement for pitch control fails, then the other panel can be used as a backup elevator, as illustrated in Fig. 8. Similarly, we have a backup rudder for yaw control and a backup aileron for roll control.

C. Attitude Control Logic

Because of control input constraints of small displacements, a nonlinear PID (proportional–integral–derivative) control logic (Refs. 5 and 6) is employed as follows:

$$T_x = -\underset{U}{\text{sat}}\left\{K\underset{L}{\text{sat}}[(\theta_x - \theta_{xc}) + \frac{1}{\tau}\int(\theta_x - \theta_{xc})] + C\dot{\theta}_x\right\}$$

$$T_y = -\underset{U}{\text{sat}}\left\{K\underset{L}{\text{sat}}[(\alpha - \dot{\alpha}_c) + \frac{1}{\tau}\int(\alpha - \alpha_c)] + C\dot{\alpha}\right\}$$

$$T_z = -\underset{U}{\text{sat}}\left\{K\underset{L}{\text{sat}}[(\theta_z - \theta_{zc}) + \frac{1}{\tau}\int(\theta_z - \theta_{zc})] + C\dot{\theta}_z\right\}$$

where U is the maximum control torque available in each axis. A variable limiter in the attitude-error feedback loop has the self-adjusting saturation limit L as

$$L = (C/K)\min\left\{\sqrt{2a|e|}, |\omega|_{\max}\right\}$$

where e is the attitude error, $|\omega|_{\max}$ is the specified maximum slew rate, and $a = U/J$ is the maximum control acceleration for each axis. Detailed discussions of this nonlinear PID control logic can be found in Refs. 5 and 6.

In terms of the standard notation for PID controller gains, K_P, K_I, and K_D, we have

$$K_P = K, \qquad K_I = K/\tau, \qquad K_D = C$$

The PID controller gains are determined as

$$K_P = J\left(\omega_n^2 + 2\zeta\omega_n/\tau\right), \qquad K_I = J\left(\omega_n^2/\tau\right)$$

$$K_D = J(2\zeta\omega_n + 1/\tau)$$

and the time constant τ of integral control is selected as $\tau \approx 10/(\zeta\omega_n)$.

Instead of the control logic of using attitude-error angles, quaternion-feedback control logic in Ref. 6 can also be employed if an attitude determination system provides attitude-error information in terms of quaternions.

Table 2 Attitude control characteristics of ST6 sail with panel translation and rotation

Characteristic	Value
Roll inertia	$I_x = 6000\ \text{kg}\cdot\text{m}^2$
Pitch inertia	$I_y = 3000\ \text{kg}\cdot\text{m}^2$
Yaw inertia	$I_z = 3000\ \text{kg}\cdot\text{m}^2$
Thrust modulation	$0 < F < 11$ mN
Thrust pointing range	$\alpha_{\max} > \alpha > 0$
Thrust pointing accuracy	± 1 deg ($3\,\sigma$)
Maximum turn rate	0.02 deg/s
cm/cp uncertainty	± 0.25 m (max)
Maximum sun angle	$\alpha_{\max} = 60$ deg
Aileron deflection	$\delta_a = \pm 1$ deg (max)
Elevator deflection	$\delta_e = \pm 0.5$ m (max)
Rudder deflection	$\delta_r = \pm 0.5$ m (max)
Maximum thrust	$F_{\max} = 11.6$ mN
Control force	$f_{\max} = F_{\max}/4 = 2.9$ mN
Roll control torque	$T_x = \pm 1.34$ e-3 N · m (max)
Pith control torque	$T_y = \pm 1.45$ e-3 N · m
Yaw control torque	$T_z = \pm 1.45$ e-3 N · m
Roll acceleration	$a_x = \pm 13.0$ e-6 deg/s^2
Pitch acceleration	$a_y = \pm 28.1$ e-6 deg/s^2
Yaw acceleration	$a_z = \pm 28.1$ e-6 deg/s^2
Control bandwidth	7e-4 rad/s
Structural mode	$\approx$0.1 rad/s
Actuator bandwidth	$>$0.07 rad/s
Actuator nonlinearity	Stiction/friction (TBD)

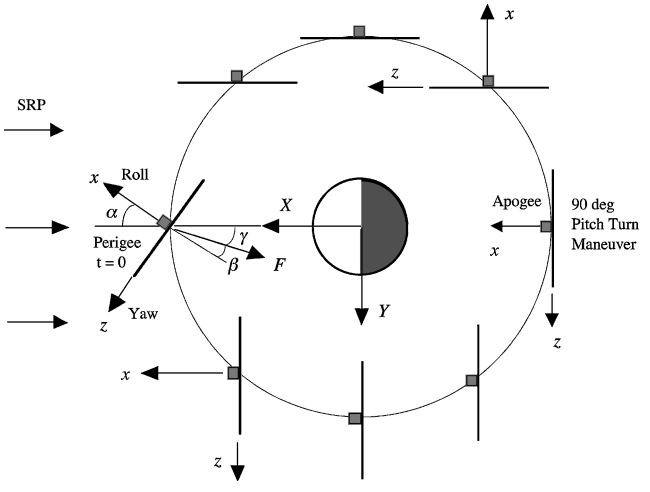

Fig. 9 Ideal orbit-raising sail-steering profile that requires two rapid 90-deg pitch maneuvers. (Because of near-zero control torque when $\alpha > 60$ deg, two 50-deg pitch maneuvers are to be performed at perigee and apogee.)

D. Attitude and Orbit Control Simulation Results

To validate the concept of propellantless space propulsion using solar sails, it is proposed that propellantless orbit-raising maneuvers be flight-tested. The proposed propellantless attitude control system will provide proper sail-attitude control and thrust-vector steering to accomplish such a primary objective.

For a solar sail demonstration mission in an Earth-centered orbit, it is important to be in a flight regime (>2000 km altitude) where the solar-pressure force is much greater than the aerodynamic drag. To meet cost constraints, the main launch options may be as a secondary payload on a commercial or government launch, or from the Space Shuttle with an additional chemical propulsion system to get into a higher orbit. A sail validation mission may include spiraling out to increase the orbital radius, changing orbit inclination, or demonstrating a levitated orbit (Ref. 1).

In order to achieve good ground-station visibility with a limited number of stations, to avoid eclipses, and to provide the most likely mission design consistent with a ride as a secondary payload, a geosynchronous orbit was considered in Ref. 1. More specifically, the geostationary disposal orbit was selected, which is geosynchronous orbit (GEO) + 300 km. This is to avoid interference with geostationary satellites.

As illustrated in Fig. 9, a simple "on-off switching" orbit-raising flight-control experiment can be conducted for such a sail flight validation mission in a geosynchronous orbit. The sail is oriented

Table 3 Simulation conditions

Condition	Value
Initial attitude errors	10 deg
Initial attitude rates	0.01 deg/s
Pitch turning rate constraint	0.02 deg/s
cm/cp offset uncertainty	0.25 m
Control saturation	$\delta_a = \pm 1$ deg
	$\delta_e, \delta_r = \pm 0.5$ m

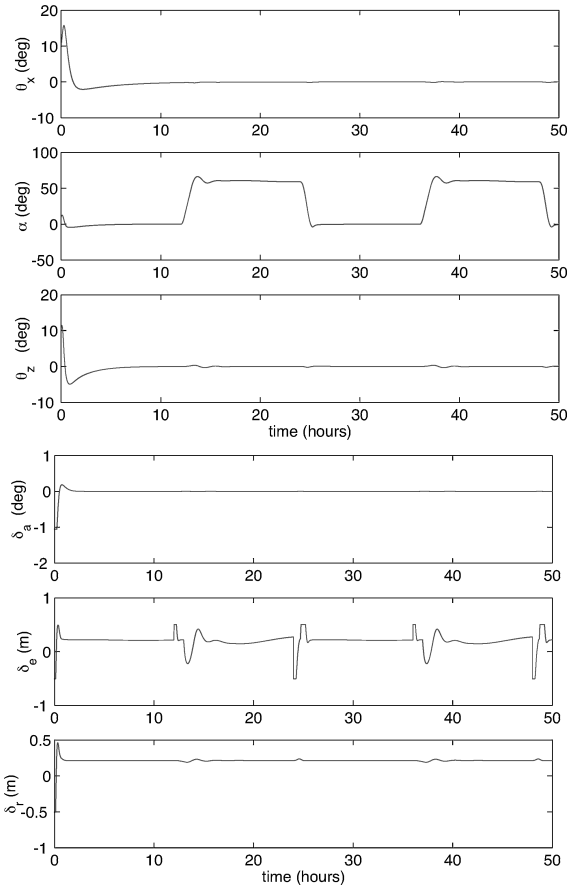

Fig. 10 Attitude and orbit control simulation results.

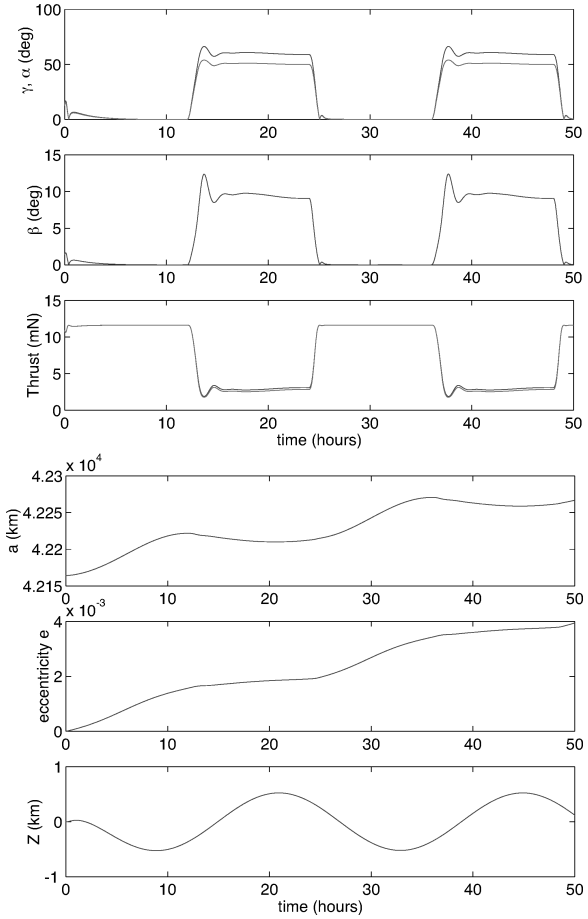

Fig. 11 Attitude and orbit control simulation results (continued).

to face the sun when the sail is moving away from the sun, but it is oriented edgewise toward the sun when the sailcraft is moving sunward. Such a simple steering profile requires two rapid 90-deg pitch maneuvers per orbit. Note that in an Earth-centered orbit, almost no orbital energy can be gained when a sailcraft is flying sunward. More sophisticated orbit-raising, sail-steering profiles can also be employed; however, the performance improvement over the simple steering profile is quite marginal in the presence of practical constraints.

The overall characteristics of the proposed attitude control system employing sail-panel translation and rotation for such a sail-flight validation mission in a geosynchronous orbit are summarized in Table 2. An attitude control bandwidth of $\omega_n = 0.0007$ rad/s, which is 10 times the geosynchronous orbital rate, is selected.

Attitude and orbit control simulation results for the simple orbit-raising sail-steering profile illustrated in Fig. 9 are shown in Figs. 10 and 11. The simulation conditions are summarized in Table 3. Simulation results indicate that the proposed attitude control system provides proper sail steering in the presence of various physical constraints. Because of possible near-zero control torque when $\alpha > 60$ deg, two 50-deg pitch maneuvers are performed per orbit. Furthermore, the propellantless orbit-raising performance (semimajor axis increase) of $\Delta a \approx 50$ km/day is demonstrated in Fig. 11 in the presence of practical constraints provided in Tables 2 and 3. In Fig. 11, two different models of solar-radiation-pressure force, described in Sec. 3.1, are also illustrated. The proposed control system was robust to those different models.

Although the feasibility of solar sail attitude control by shifting and tilting sail panels has been demonstrated here, the proposed control system will require precision control mechanisms for reeling in or paying out the inboard tether from the spool. It will also require precision twisting of the spreader bars at the end of the booms. Although the essential idea behind all "cm/cp methods" appears simple, there are challenging hardware implementation problems to be solved.

V. Conclusions

Various dynamic models and control design options have been presented for sailcraft attitude control systems design and tradeoffs. Particular emphasis was placed on various control design options for countering the significant solar-pressure disturbance torque caused by an uncertain offset between the center of mass and the center of pressure. A 40×40 m, 160-kg sailcraft with a nominal solar pressure force of 0.01 N, an uncertain cm/cp offset of ± 0.1 m, and moments of inertia of (6000, 3000, 3000) $\text{kg} \cdot \text{m}^2$ was chosen as a baseline sailcraft to illustrate the various concepts and principles involved in dynamic modeling and attitude-control design. The study results will provide the sail mission designer with options and approaches to meet the various requirements of near-term sails as well as future advanced solar sails.

Acknowledgments

This research has been supported by JPL Contract 1228156 from the Solar Sail Technology Working Group of the NASA In-Space Propulsion Program. It was also in part supported by the New Millennium Program Space Technology 7 Solar Sail Concept Study Project. The author thanks H. Price at the Jet Propulsion Laboratory, L. Johnson at NASA Marshall Space Flight Center, and C. Moore at NASA Langley Research Center for their support for this research. The various solar sail control concepts studied in this paper are currently being further investigated for a solar sail ground validation experiment of the NASA In-Space Propulsion program, managed by G. Garbe and E. Montgomery at NASA MSFC. The author also thank the reviewers and the Associate Editor, Panagiotis Tsiotras, for their comments and suggestions, which significantly improved the quality of this paper.

References

[1]Price, H. W., Ayon, J., Buehler, M., Garner, C., Klose, G., Mettler, E., Nakazono, B., and Sprague, G., "Design for a Solar Sail Demonstration Mission," Space Technology and Applications International Forum (STAIF 2001), Albuquerque, NM, Feb. 2001.

[2]Murphy, D. M., Murphey, T. W., and Gierow, P. A., "Scalable Solar Sail Subsystem Design Considerations," AIAA Paper 2002-1703, April 2002.

[3]Garbe, G., and Montgomery, E., "An Overview of NASA's Solar Sail Propulsion Project," AIAA Paper 2003-4662, July 2003.

[4]Wie, B., "Solar Sail Attitude Control and Dynamics: Part 1," *Journal of Guidance, Control, and Dynamics*, Vol. 27, No. 4, pp. 526–535.

[5]Wie, B., and Lu, J., "Feedback Control Logic for Spacecraft Eigenaxis Rotations Under Slew Rate and Control Constraints," *Journal of Guidance, Control, and Dynamics*, Vol. 18, No. 6, 1995, pp. 1372–1379.

[6]Wie, B., Heiberg, C., and Bailey, D., "Rapid Multi-Target Acquisition and Pointing Control of Agile Spacecraft," *Journal of Guidance, Control, and Dynamics*, Vol. 25, No. 1, 2002, pp. 96–104.